Pergamon

1359-6454(95)00411-4

Acta mater. Vol. 44, No. 7, pp. 2891–2900, 1996

Published by Elsevier Science Ltd

1359-6454/96 $15.00 + 0.00

THREE-DIMENSIONAL SIMULATION OF DISLOCATION–CRACK INTERACTIONS IN B.C.C. METALS AT THE MESOSCOPIC SCALE

B. DEVINCRE† and S. G. ROBERTS

Department of Materials, Oxford University, Parks Road, Oxford OX1 3PH, England

(Received 6 September 1995)

Abstract—A simulation of the dynamics of dislocation loops emitted at or close to a crack tip in b.c.c. metals is presented. The model simulates the growth of the crack tip plastic zone. The elastic (shielding) interactions between the plastic zone and the crack are calculated as a function of time and temperature, allowing modelling of the increase in fracture toughness with temperature (i.e. the brittle–ductile transition near the lower shelf). The three-dimensional nature of the model allows for the first time study of the differences between dislocations of blunting and non-blunting types, i.e. in configurations where the emitted dislocation glide plane either does or does not contain the crack tip. We found that the blunting configuration induces a localised shielding of the crack close to the dislocation sources, but is not sufficient to give strong toughness increases. Conversely, non-blunting geometries produce more efficient shielding of the crack and are characterised by a slower extension of the plastic zone far from the crack tip. The model also demonstrates the importance of the density of dislocation sources along the crack tip in determining the form of the brittle to ductile transition. *Crown copyright © 1996*

1. INTRODUCTION

In many semi-brittle materials the evolution of the crack tip plastic zone and the elastic interactions between dislocations and cracks control the fracture behaviour and the brittle to ductile transition (BDT). Extensive experimental and theoretical work has focused on this problem (see for a review article Ref. [1]).

Rice and Thomson [2] distinguished between intrinsically ductile and brittle materials according to whether the nucleation of a dislocation loop from a crack tip subjected to a stress is spontaneous or involves surmounting an energy barrier. This model, though, gave little scope for consideration of the temperature variation of fracture stress. Later models [3, 4] have suggested that the nucleation of dislocations at the crack tip is not intrinsically difficult, but rather that the BDT is controlled by the dislocation glide mobility. This is now supported by experimental evidence from a wide range of materials, where the activation energy for the BDT is consistently found to equal that for dislocation glide.

Some materials (e.g. silicon, sapphire) normally exhibit a sharp brittle–ductile transition; that is, the stress to fracture stays nearly constant (at the low temperature K_{Ic}) below the BDT temperature. At the BDT, the stress to fracture rises very rapidly over a narrow temperature range (5°C or less). Other materials (e.g. b.c.c. metals) normally exhibit a soft brittle–ductile transition; below the BDT the stress to fracture rises steadily with increasing temperature over a wide temperature range (typically 100–150°C). In both cases, above the BDT temperature, specimens yield and do not fracture. Experiments [5] and modelling [6] show that a sharp transition is associated with a crack with very few widely spaced dislocation sources, and that a soft transition is associated with a crack with many closely spaced dislocation sources.

When dislocation sources at or close to the crack tip start to operate at low values of applied stress intensity (K_{app}), the time dependence of the crack tip stress intensity depends on the rate at which the dislocations in the plastic zone can move away from the crack tip [6, 7]. When a dislocation is nucleated, it shields the crack tip from K_{app} very effectively and exerts a strong back-stress on the dislocation source, preventing the emission of the next dislocation. As the dislocation glides away, the shielding effect on the crack tip and the back-stress on the source decrease. The dislocation source can only nucleate a new dislocation when the previously emitted dislocation has moved some distance away. The dislocation nucleation process is thus controlled by dislocation glide. The BDT is "soft", the fracture stress increases gradually with increasing temperature and is accompanied by increasing amounts of dislocation activity around the crack tip before fracture occurs. The present work is focused on this type of behaviour.

†Permanent address: LEM, CNRS-ONERA, BP 72, 92322 Chatillon, France.

In the past few years, direct simulations of the plastic zone dislocation dynamics around a crack tip have been used to interpret and predict the temperature dependence of the fracture toughness of single crystal [4, 7–9]. These simulations were restricted to modelling two-dimensional approximations to the plastic zone (i.e. straight dislocations parallel to a semi-infinite crack tip), since:

(1) dislocations and cracks interact over very long ranges, and as the number of dislocations rises, a rapidly increasing number of mathematically complex interactions must be calculated;
(2) the equilibrium state is never achieved or even approached, as the simulations (of real test cycles) always use a rising stress intensity factor; and
(3) some physical quantities, e.g. the effective crack tip stress intensity factor and the dislocation image forces induced by the presence of the crack surfaces [10], are easily formulated in two dimensions using complex elastic potentials [1]. Computation of these quantities in three dimensions is difficult, and requires approximations discussed below.

The development of three-dimensional simulations is desirable so as to test the sensitivity of the existing models to dislocation properties neglected or oversimplified in two dimensions. For example, in real plastic zones, dislocation line curvature gives rise to line tension effects and the dislocation velocity varies with the dislocation character (screw or edge) at different parts of each dislocation loop. In general, glide planes do not contain or are not parallel to the crack tip, as is necessarily the case for two-dimensional models. Thus, the two-dimensional models, while very successful so far in explaining and predicting the BDT, could be inaccurate in some respects.

This paper reports a first attempt at a three-dimensional simulation of plastic flow around a crack. Molybdenum was taken as a representative b.c.c. metal since its elementary dislocation properties, including stress/temperature/velocity relations, are fairly well known [11–14]. The paper is organised as follows: Section 2 presents the main ingredients used in the simulation, as well as a description of the validation tests performed to fit the modelling parameters. Section 3 presents results of simulated tests; these consist of comparisons of the crack tip shielding efficiency with different dislocation emission conditions and at different temperatures. In particular, the influence of the dislocation glide plane orientations and the coordinated effects of multiple dislocation sources were studied. Finally, the results are discussed and summarised in Section 4.

2. SIMULATION METHOD

2.1. *Space and dislocation discretisation*

This simulation derives from the one developed some years ago for modelling plastic flow in f.c.c. metals at the mesoscopic scale [15, 16]. It is based on discretized dislocation dynamics, at an intermediate scale of modelling between atomic simulations and finite element methods. Dislocations are viewed as a series of screw and edge segments connected at the nodes of a simulation lattice tiling an isotropic elastic continuum. This "screw-edge" dislocation line model (discussed in detail by Devincre and Condat [17]) allows for a good three-dimensional description of the dislocation stress field at the appropriate scale. Exact modelling of the line curvature effects would imply a large increase in the number of dislocation segments, with a consequent rapid increase in computation time, so the simplest topological solution is adopted; curved dislocation loops are replaced by equivalent square loops (Fig. 1.).

The simulation lattice has the same cubic geometry as the crystallographic lattice of molybdenum. The simulation lattice parameter, a, was set equal to Burgers vector length ($b = 0.272$ nm). Such a small simulation network lattice parameter was necessary to enable accurate simulation of the dynamics of the

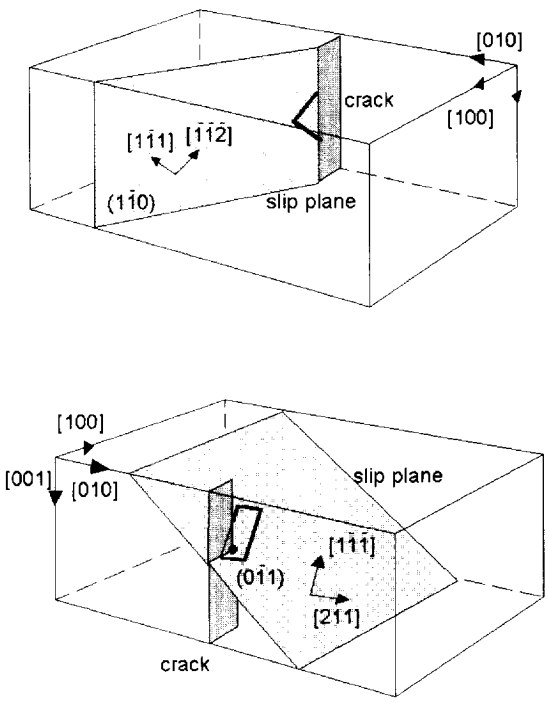

Fig. 1. The blunting and non-blunting configurations modelled in the three-dimensional simulation: (a) the "blunting" configuration where the emitted dislocation glide plane is normal to the crack tip. One half of the dislocation loop is eliminated at the crack surface, where it will blunt the crack tip; (b) the "non-blunting" configuration where the dislocation glide plane is tilted and no strong blunting effect is expected.

dislocation pile-ups close to the crack tip where the internal stress field variations are rapid (in the earlier simulations of general plasticity in a uniform stress field in copper, the network could have a much larger lattice parameter than b). The three-dimensional nature of the simulation lattice also allowed us to reproduce the anisotropy in velocity of edge and screw dislocation characters. In b.c.c. metals at low temperature, dislocations glide on $\{110\}$ planes with Burgers vector directions equal to $\langle 111 \rangle$. In our model the dislocation displacement was restricted to these lattice directions.

The simulation box, of size $320 \times 160 \times 160$ μm, is large enough to minimise boundary effects and to study a realistic plastic zone, in both size and dislocation density. The simulation is terminated when a screw dislocation reaches the edge of the box. Inside the simulation box, a semi-infinite crack is modelled with its cleavage plane normal to the applied stress direction [010]. The crack is on a (100) plane with its straight tip in the [001] direction and a crack length, $l = 20$ μm (Fig. 1). These correspond fairly closely to the experimental arrangements used by Ellis [11].

Since the details of the dislocation emission process at the crack tip are experimentally unknown, this part of the simulation was simplified as much as possible. Sources were modelled as loops of radius X_s, with the centre of the loop at the crack tip. We assumed that a dislocation can be nucleated at a source and move away from the tip provided the stress in the dislocation glide plane is sufficient to expand a notional loop at the source (i.e. the force on the dislocation line is everywhere at least enough to prevent the loop collapsing). Reducing X_s changes the initial size of the loop and thus increases the interaction forces between opposite parts of the dislocation loop. At the same time, the dislocation line is everywhere closer to the crack tip and the expansion force on the dislocation loop increases. For these reasons, the overall force on the dislocations in the source loop does not vary rapidly with X_S. During these simulations, X_S was set equal to $100\,b$, resulting in the emission of the first dislocation loop at an applied stress intensity factor of about $1.5\ \mathrm{MPa}\sqrt{\mathrm{m}}$.

Figure 1 shows the two geometries modelled, the "blunting" and the "non-blunting" configurations ("BC" and "NBC", respectively). In the blunting configuration the dislocation glide plane contains the crack tip. Here, only emission of dislocation half-loops needs to be considered, since the rest of the dislocation loop is eliminated at the crack surface. The dislocation line annihilation at the crack surfaces results in crack tip blunting. The effect of the blunting on the crack tip stress was not studied here. This kind of emission geometry is experimentally rare [18], but is useful for comparison with the existing two-dimensional models.

In the non-blunting configuration the dislocation glide planes are tilted with respect to the crack plane. The geometry corresponds to dislocation loops surrounding the crack tip and cutting the crack surface. We assumed a symmetrical displacement of the dislocation line on each side of the crack surface. Although not quite satisfactory, this condition was used in the absence of an exact description of the stress state at the free surface of the crack; it is a reasonable approximation as forces on the segments were always computed far from the free surface.

2.2. *Dislocation dynamics*

The main step in the simulation of dislocation dynamics is the computation of the effective force acting at the centre of each segment. This is the sum of:

(1) the force due to the externally applied stress. This increases during the simulation, with a constant stress rate, 10^{-4} G/s, compatible with experimental conditions. G, the shear modulus, is equal to 130 GPa for molybdenum;
(2) the force resulting from the crack stress field. This term was calculated using the Peach–Koehler equation and the plane strain mode I crack stress tensor solution [1];
(3) the force due to the interactions of a given segment with all other segments belonging to the same dislocation or to different dislocations. This term was calculated using the Peach–Koehler equation, summing up the stress field of all other dislocation segments at the centre of the segment being considered. The stress field tensor expression used was derived from the de Wit solution [17, 19]. This is the most time-consuming part of the simulation; it was optimized by assuming that elastic dislocation–dislocation interactions at distances larger than 1 μm vary only slowly with time; these long-distance contributions were thus recalculated at intervals of 10 simulation steps. This trick accelerated the speed of computation by a factor of more than three without any noticeable changes in the simulation results;
(4) the force due to the gradient of the dislocation elastic line energy, i.e. the local line tensions. This contribution is easy to obtain for the "edge-screw" dislocation line model; the method used considers the increase in dislocation line energy due to the extension of the neighbouring attached segments, as discussed in Refs [16, 17];
(5) the image forces on dislocations due to the existence of the free surfaces at the crack. This contribution, which is difficult to compute efficiently in three dimensions, needed to be simplified. We used a stress oriented in the direction of the nearest part of the crack at a

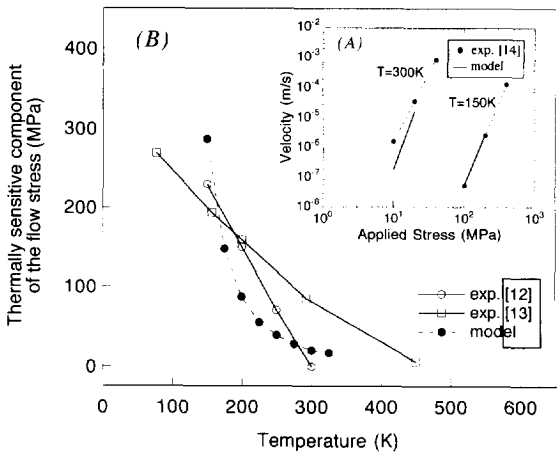

Fig. 2. Validation of the dislocation motion equation parameters [equation (2)]. Figure 2(A) shows screw dislocation velocity versus applied stress at different temperatures, with experimental results (points, dotted lines) [18] and the fit to equation (2) (solid lines). Figure 2(B) shows a comparison between experiments [16 (squares) and 17 (open circles)] and the results of modelling of the variation of the thermal sensitive part of the flow stress with temperature.

distance r, and with an amplitude equal to $\alpha Gb/r$. α is equal to $1/4\pi$ and $1/4\pi(1-\nu)$, respectively, for the screw and edge segments, where ν is Poisson's ratio.

The displacement of each dislocation segment (Δx_i) is then calculated for each time step of the simulation (of duration Δt) given the dislocation segment's velocity

$$\Delta x_i = V_i \cdot \Delta t. \tag{1}$$

The velocity/stress/temperature expression used was (for a physical justification of this expression with b.c.c. metals see, for example, Ref [20])

$$v = A\left(\frac{\tau^*}{\tau_0}\right)^m \exp\left(\frac{-\Delta U}{kT}\right) \text{ and } m = \frac{B}{T} + C \tag{2}$$

with $A = 8.608 \times 10^{-3}$ m/s, $B = 334$ K, $C = 3.4$, $U = 0.49$ eV and $\tau_0 = 1$ MPa.

In equation (2), τ^* is the resolved shear stress on the segment, ΔU is the activation energy for dislocation velocity, k is the Boltzmann's constant, m is the stress exponent of the velocity and τ_0 a stress normalization constant. A, B and C are parameters fitted to experimental data for dislocation velocity in molybdenum [11]. The accuracy of this fit for our three-dimensional model was checked by comparison with experiments. Figure 2 shows simulated and experimental [12–14] results for the temperature dependence of the velocity of an isolated dislocation [Fig. 2(a)] and the variation of the thermally-activated part of the flow stress of single crystals [Fig. 2(b)] (see Ref. [16] for details of the simulation procedure used). Simulations of the flow stress were made with an initial dislocation density of 10^{12} m^{-2} and neglecting forest interactions to produce only for the thermally-activated part of the flow stress. The calculation results are in good agreement with experiments.

For edge dislocations, the velocity used was that of an equivalent screw dislocation multiplied by a factor of 10. This is a reasonable approximation, consistent with experimental data [14].

The simulation time step (Δt) used was the maximum time interval that was possible without reducing the stability of the simulation results. Care was needed in the selection of Δt, since the different parts of the dislocation loops can glide at very different speeds in the strong stress field gradient near the crack. Δt varied with temperature and ranged from 0.1 to 5 μs. The maximum total simulated time was a few seconds, which is equivalent to a few millions of simulation steps.

At the beginning of each cycle of the simulation, the program checks for the possibility of emission of new dislocation loops from the sources and for possible dislocation reactions. Since dislocations coming from the same kind of sources have the same Burgers vector, only annihilations of dislocation lines of opposite sense need to be considered. This dislocation reaction was performed by elimination of the segments in each loop in the region of their superposition between nodes of the simulation lattice.

2.3. Computation of the crack tip stress intensity factor

The purpose of the simulation is to study the time evolution of the crack tip stress intensity, modified from the applied stress intensity by the shielding effect of the dislocations emitted by sources distributed along the crack tip. Unfortunately, an analytical solution for the crack stress intensity factor including the elastic interactions between dislocations and a crack does not exist for the three-dimensional case. A rigorous treatment of this problem would involve finding the crack surface shape which would simultaneously relax the applied and dislocation stress fields. Even if this were possible, the calculation would have to be done at many points of the crack surface at each step of the simulation. This would be too costly in computer time. A simplified approach must be used.

In two dimensions, the effective stress intensity factor at a crack tip, K_{eff}, is given [1] by

$$K_{\text{eff}} = K_{\text{app}} + \sum_i K_{\text{d}}^i. \tag{3}$$

The first term of equation (3), K_{app}, is the crack stress intensity factor equal to

$$K_{\text{app}} = \sigma_{yy}\sqrt{2\pi l} \tag{4}$$

where σ_{yy} is the applied stress normal to the cleavage plane, and l is the crack depth. The second term of

equation (3), K_d^i, is the shielding effect of each dislocation i on the crack and is given by

$$K_d^i = \frac{Gb}{(1-\upsilon)\sqrt{2\pi r_i}}\Psi(\theta, \mathbf{b}) \tag{5}$$

where r_i and $\Psi(\theta, \mathbf{b})$ are, respectively, the distance from the dislocation i to the crack tip and the angular dependence of the dislocation shielding. A comparison of this last function with the usual expression for the dislocation stress field in an infinite perfect crystal [21] suggests that a local approximation for the crack tip shielding is possible if we know the stress field contribution associated with each dislocation

$$K_d^i \propto \sqrt{Gb|\sigma_{yy}^i|\Psi(\theta, \mathbf{b})}. \tag{6}$$

σ_{yy}^i is the dislocation stress field normal to the cleavage plane at the tip coordinate, r_i, in the absence of the crack. The extension of this local shielding approximation to three dimensions is restricted by two important difficulties:

(1) σ_{yy}^i is not a constant quantity along the crack tip and must be calculated at different points along the tip;
(2) the angular dependence $\Psi(\theta, \mathbf{b})$ for a dislocation segment in three dimensions is unknown. We assumed this dependence to be reflected by the spatial variation of the stress field from each dislocation segment close to the crack tip. The stress field of the segments far from the crack tip varies smoothly in space and the shielded regions are necessarily where σ_{yy}^i opposes the crack tip opening. Conversely, anti-shielding regions are where σ_{yy}^i locally increases the applied stress on the crack.

During the simulations, the computation of dislocation shielding was based on this simplification. It was calculated at each time step and at equidistant points along the crack tip using the dimensionless function

$$S = \frac{K_{eff}}{K_{app}} = \frac{\sigma_{yy}\sqrt{2\pi l} + \sum_i \sqrt{Gb|\sigma_{yy}^i|}\cdot\mathrm{sign}(\sigma_{yy}^i)}{\sigma_{yy}\sqrt{2\pi l}}. \tag{7}$$

Validation of this simple function was performed by comparison with the exact calculation in two dimensions [equation (3)]. We tested the shielding, S, at positions around the crack tip, of a long straight dislocation, parallel to the crack and cutting the two opposite sides of the simulation box. Calculations of S at points along the crack tip using equation (7) were found to be completely consistent with the two-dimensional exact computation of K_{eff}/K_{app}. S fluctuates strongly at each dislocation emission. In our computations, these variations were smoothed by continuously averaging S over a thousand successive time steps.

3. SIMULATION RESULTS

3.1. The blunting configurations (BC)

3.1.1. Operation of a single dislocation source. Simulations were initially performed using the geometry shown in Fig. 1(a), which can be more easily compared to existing two-dimensional models.

As a first step, the operation of only one source at the middle of the crack tip was considered. Figure 3 shows an example of a plastic zone for this type of source. During the crack loading, emitted half-loops rapidly expand over a small "dislocation free zone" close to the source and then expand asymmetrically inside the crystal. The dynamics of this are controlled by the different mobilities of the edge and screw dislocation segments. The edge dislocations propagate rapidly, creating a large plastic zone in front of the crack tip. Screw dislocations form a dense reversed pile-up with the maximum dislocation density very close to the source (Fig. 3). Back stresses on the source from the screw dislocations control the source's emission rate. The high mobility of the edge dislocations is the origin of the dislocation free zone.

The dislocation shielding along the crack tip follows this asymmetry of the plastic zone expansion. The region of the crack tip within the loops is shielded by the dislocations (i.e. the stress intensity here is lower than the applied K), while outside the loops the crack tip is anti-shielded (i.e. the stress intensity here is higher than the applied K). At low temperatures (Fig. 4), since the mobility of the screw dislocations is very small, only half of the crack where edge dislocations operate is shielded. The screw dislocation pile-up does not give efficient shielding of the crack, since only a small fraction of the length of these dislocations is close to the crack. The total shielding is large only near the dislocation source. At higher temperatures (Fig. 5), dislocations move faster, the source emission rate goes up and the length of the crack which is shielded is larger. However, the plastic zone is far from the crack and mainly

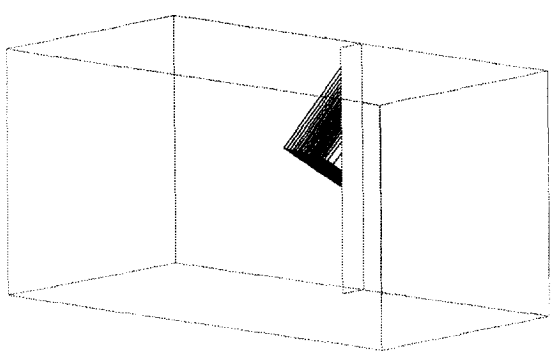

Fig. 3. Instantaneous image of the three-dimensional simulation with one active blunting dislocation source at the middle of the crack, at $T = 175$ K and $t = 0.8$ s. The geometry is as in Fig. 1(a). About 20 dislocation loops have been emitted. Note the compact reverse pile-up of screw dislocations close to the dislocation source.

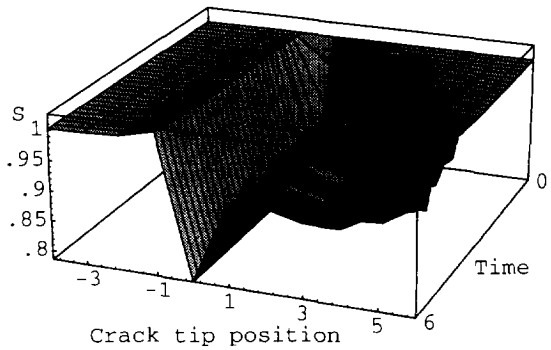

Fig. 4. Time variation of the plastic zone shielding with one blunting dislocation source at $T = 125$ K. Simulation time varies from $t = 0$ at the back of the figure to $t = 6$ s at the front. The local shielding function S defined in the text is computed at various points along the crack tip. The dislocation source is at position 0 on the crack tip and the distance between each of the computing points is $5000\,a = 1.36\,\mu$m. Positive positions are on the side of the source where edge dislocations are active.

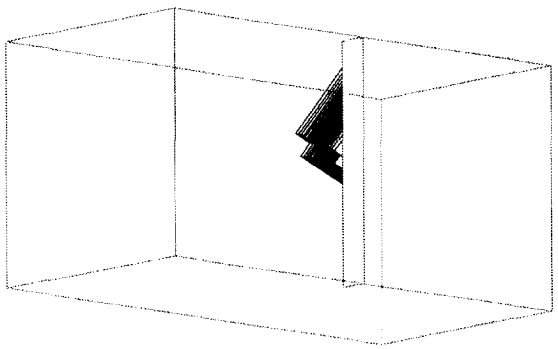

Fig. 6. Instantaneous image of the three-dimensional simulation with two blunting dislocation sources separated by $\sim 8\,\mu$m, at $T \approx 175$ K and $t = 0.8$ s. About 20 dislocation loops have been emitted from each source. Note that the screw dislocation density in the centre of the plastic zone is small since most of these dislocations have been annihilated.

composed of edge dislocations. At distances of more than a few microns from the dislocation source the shielding is poor (less than 10% of the applied stress intensity).

3.1.2. Operation of multiple dislocation sources. In the two-dimensional models, either

(1) the whole crack front is uniformly shielded, or,
(2) as a first approximation to the real situations in which a limited number of sources are distributed along the crack front, a critical distance parameter, d_{crit}, is introduced, corresponding roughly to the spacing between sources. Each dislocation's shielding is "switched on" when it has gone more than d_{crit} from the source; this is to approximate to the dislocations being effective when they have combined to form large loops shielding the whole crack front (see e.g. Fig. 5 of Ref. [7]).

To allow the comparison of the three-dimensional simulations to these two-dimensional ones, and to the real crack tip source configurations, multiple crack tip sources were used. Firstly, we considered the operation of two BC sources separated by 8.16 μm ($300a$) along the crack tip. With this geometry, the emitted dislocations from the two sources eventually meet and combine to form an array of larger loops extended in the crack tip direction, similar to the assumptions made in the use of d_{crit} in the two-dimensional models. Figure 6 shows such an array of dislocations after the same simulation time as in Fig. (3). The emission rate was found to be much higher than for isolated sources (see Fig. 9). This is because when more than one BC source exists, annihilation of the dislocations between the sources eliminates a large part of the screw dislocation density; the back stress at the sources is lowered and so dislocation loops are emitted more frequently. The

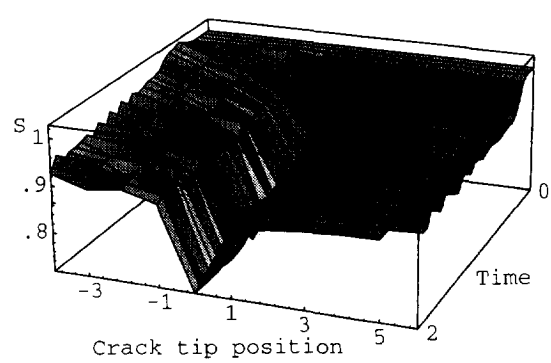

Fig. 5. Time variation of the plastic zone shielding with one blunting dislocation source, as in Fig. 4, but at $T = 175$ K. Simulation time varies from $t = 0$ at the back of the figure to $t = 2$ s at the front. The crack is shielded on each side of the dislocation source since the screw dislocation lines are much more mobile than at 125 K. Nevertheless, the dislocation shielding far from the source is weak, and tends to a constant fraction ($\sim 10\%$) of applied K.

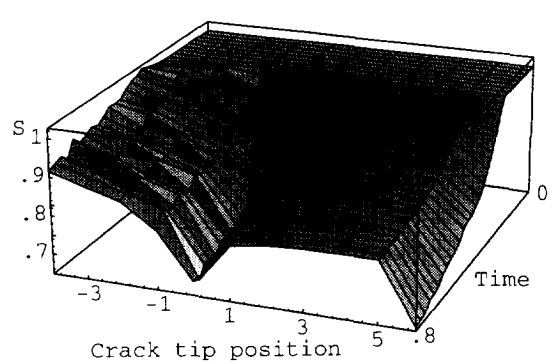

Fig. 7. Time variation of the plastic zone shielding with two blunting dislocation sources (at $y = 0$ and 6) at $T = 175$ K. Simulation time varies from $t = 0$ at the back of the figure to $t = 0.8$ s at the front. The crack is shielded between the two dislocation sources.

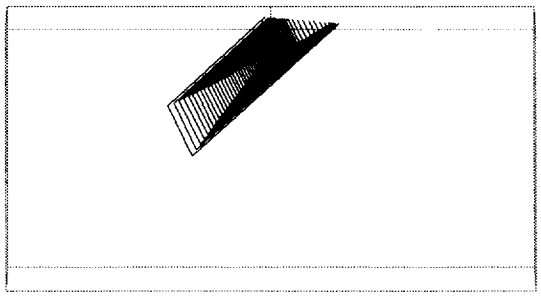

Fig. 8. Instantaneous image of the three-dimensional simulation with one non-blunting dislocation source at the middle of the crack at $T = 175$ K and $t = 4$ s. The geometry is as described in Fig. 1(b). About 40 dislocation loops have been emitted. Two dense screw dislocation pile-ups are formed on each side of the crack.

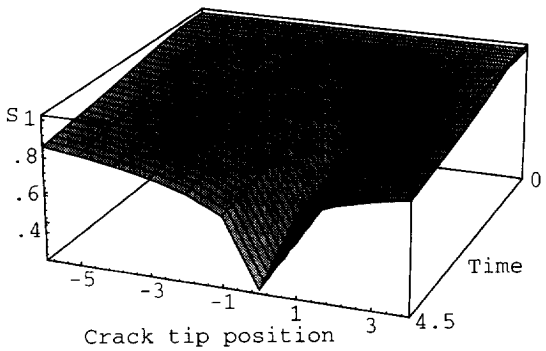

Fig. 10. Time variation of the plastic zone shielding with one non-blunting dislocation source at $T = 175$ K. Simulation time varies from $t = 0$ at the back of the figure to $t = 4.5$ s at the front. The dislocation shielding of the crack is relatively strong both close to and distant from the source. Shielding increases steadily during the simulation, with no "plateau" as for the blunting sources (Figs 4 and 7).

dependence of dislocation shielding on time and position between the two sources is shown in Fig. 7. The shielding is small, since most of the plastic zone, dominated by edge dislocations, is far from the crack.

In our model, the mobility of the edge segments [taken as 10 times that of the screw velocity calculated in equation (2)] is somewhat slower than the real velocity at the stresses and temperatures used here. The computed shielding effect is thus likely to be larger than the real one.

Reduction of the distance between the sources cannot be made without prohibitive increases in the computing time needed, because of the reduction in the simulation time step. However, varying the source spacing within the range of a few microns is not expected to change these simulation results substantially.

3.2. *The non-blunting configurations (NBC)*

3.2.1. Single dislocation source. The next step was to extend the simulations to the more general glide plane geometry shown in Fig. 1(b): the non-blunting configuration. We studied first a crack tip with only one source at its centre. The shape of the plastic zone at $T = 175$ K is shown in Fig. 8. Dislocation loops

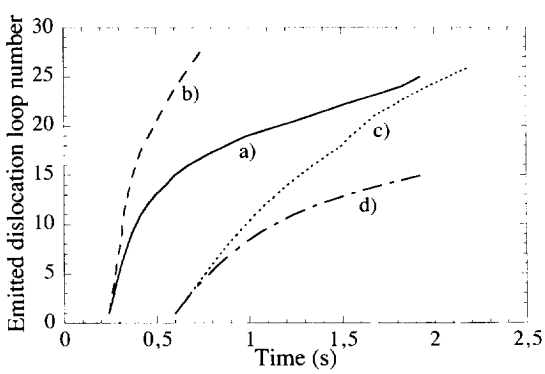

Fig. 9. Time variation of the dislocation source emission rate for different simulation configurations. (a) Single blunting source; (b) two blunting sources; (c) single non-blunting source; (d) six non-blunting sources of two characters.

are extended in the [1$\bar{1}\bar{1}$] screw direction and form two dense reverse pile-ups on each side of the crack tip.

With an initial (nucleating) loop radius identical to that of the BC simulations, the first dislocation emission appears at a slightly higher stress intensity factor than for the BC case. This small increase arises from (a) an increase of the elastic interactions between opposite parts of the loop (in the BC only a half loop exists); (b) a smaller resolved stress in the dislocation glide plane from the crack tip stress field. Nevertheless, Fig. 9 shows that the rates of dislocation emission for an isolated source in the BC and NBC configurations are very similar. This is because of the dominating influence of the low screw dislocation mobility.

At low temperatures, few dislocations are emitted which stay close to the source. The dislocation shielding is limited to a small region of the crack near to the dislocation source. At higher temperatures (for the same simulation time), the plastic zone size is larger; its shielding effect is stronger and extends over a greater distance along the crack tip.

Comparison of Figs 5 and 10 shows two important differences between BC and NBC shielding. Firstly, close to the dislocation source, the NBC shielding is stronger since there are two screw dislocation pile-ups. Secondly, far from the source, the shielding effect in the NBC decreases rapidly since the dislocation glide plane is inclined to the crack plane. Nevertheless, the shielding intensity at any point on the crack tip increases continuously and no "saturation" occurs as in the BC case. During the NBC simulations, the plastic zone contains mostly screw dislocations, which provide efficient shielding since these dislocations are close to the crack.

Similar simulations were performed with a different type of NBC source. The Burgers vector direction was [$\bar{1}\bar{1}$1] and the glide plane was (011). The plastic zone was again found to extend in a

crystallographic direction parallel to the direction of the screw dislocations, and the dynamical and shielding properties were identical to those of the previous NBC configuration simulations.

3.2.2. Multiple sources. The final series of computations was for an evenly spaced distribution of NBC dislocation sources along the crack tip, (spacing 10,000 $a = 2.72\ \mu$m), with alternate sources of Burgers vector $a/2[\bar{1}\bar{1}1]$ and $a/2[1\bar{1}\bar{1}]$. Local reactions between dislocation lines of the two glide systems were not considered; only long-range elastic dislocation–dislocation interactions were taken into account. This simplification is justified since any dislocation reactions would be very close to the crack tip, where the stress is too high for any dislocation junctions to be stabilized. Moreover, the influence of kink formation on the dislocation mobility is negligible in comparison with the applied stress in this region.

Figure 11 shows an example of a plastic zone of this type formed at $T = 175$ K. The existence of the two glide systems allows the formation of a plastic zone which is symmetrical on each side of the crack plane; this shape of the plastic zone is very similar to some observed experimentally [18, 22].

In this configuration, the loops emitted from different sources cannot combine and the dislocation density increases more rapidly than in the multiple source BC case. There are strong elastic interactions between dislocations from different sources and a dynamical coupling of the dislocation pile-ups was observed. As shown in Fig. 9, the dislocation nucleation rate is reduced compared to the BC case. This is because the back stresses at the crack tip from the dislocations in the plastic zone stress are higher, as the emitted dislocation mobility is lowered by the strong elastic interactions inside the plastic zone and by the smaller resolved stress in the dislocation glide plane from the crack stress field.

Figure 12 shows results from the simulations for temperatures of 125, 150 and 175 K. The figure shows the time evolution of crack tip shielding at various positions along the crack front. At low temperature the shielding is localized close to the sources and there

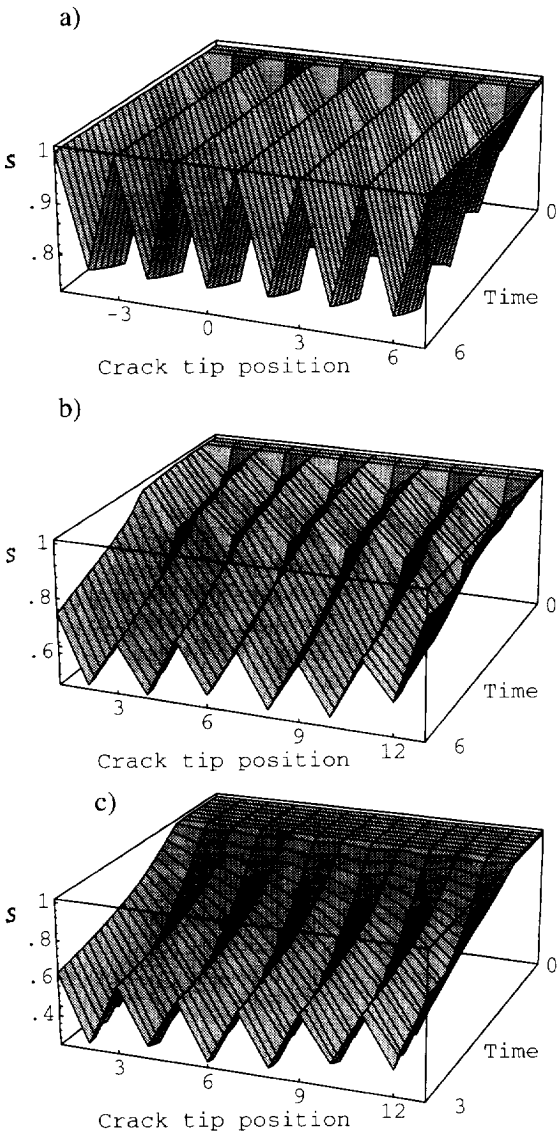

Fig. 12. Time variation of the plastic zone shielding with the dislocation source arrangement shown in Fig. 11. (a) $T = 125$ K, total simulation time, $t_{end} = 6$ s; (b) $T = 150$ K, $t_{end} = 6$ s; and (c) $T = 175$ K, $t_{end} = 3$ s. The dislocation shielding increases with temperature and is a maximum close to the sources. At high temperatures, the shape and the size of the plastic zone is such that the whole crack tip near to the sources is shielded strongly, with no shielding plateau.

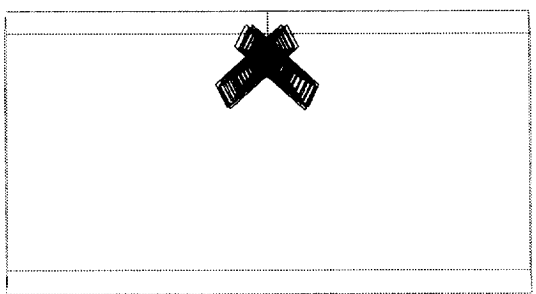

Fig. 11. Instantaneous image of the three-dimensional simulation with six active non-blunting dislocation sources, on two glide systems, evenly distributed along the crack tip, at $T = 175$ K and $t = 3$ s.

is no overlap of the shielding effect from different sources. As the temperature increases, each source emits more dislocations in a given time, the intensity of the shielding increases and the shielded regions start to overlap. With further increase in time and temperature the number of dislocations in the plastic zone increases again; the dislocations are mainly of screw character, with relatively low velocity and produce a strong shielding effect. In this case, when many non-blunting sources exist along the crack tip, the shielding effect predicted is very similar to that predicted by the two-dimensional models [6], though

now with a much more realistic simulation of the geometry of the plastic zone.

4. DISCUSSION

This article discusses the first results of a new three-dimensional simulation, at the dislocation level, of the dynamics of a crack tip plastic zone. Despite present limitations both practical (computing time) and theoretical (accurate three-dimensional formulations of dislocation shielding and image force), it is possible to model numerically the formation of the crack tip plastic zone during simulated fracture experiments. These simulations provide important results complementary to comparable earlier two-dimensional simulations.

In three dimensions, two types of source configuration can be distinguished: the blunting configuration (BC), where the crack plane and the slip plane have a line in common, and the non-blunting configuration (NBC), where they do not. In agreement with the calculations of Zhou and Thomson [23], we found that dislocation emission from BC sources is easier. This is because: (a) only a half loop must be created, while a whole loop is necessary in the NBC; (b) the BC dislocations spread out along the length of the crack tip and in a plane where the crack stresses in mode I are high, while in the NBC dislocations expand away from the crack on a glide plane where the crack stresses decrease rapidly. The co-operative behaviour of dislocations from different sources is also important. In the BC, the emission rate is high because the dislocations can annihilate between adjacent sources, mostly eliminating the screw dislocation pile-up in front of the sources. In the NBC, dislocation reactions do not reduce the density of the screw dislocations. The difference between BC and NBC configurations is small at the beginning of the simulations (i.e. for the first dislocation emissions), and increases as the plastic zone is formed and interacts elastically with the sources (Fig. 9).

If the BC is the easiest emission geometry, then one should ask why this configuration appears so rarely in experimental observations [18, 22]. The reason is probably dependent on the real geometry and crystallography of the crack tips. Real crack tips are not oriented perfectly in the emission slip plane and "BC" dislocation sources must be distributed on very closely adjacent planes. Complex reactions of dislocations of two sources will arise, rather than simple annihilations of dislocations from adjacent sources. Dipoles may form, inhibiting the operation of the sources quite strongly or the dislocations may cross-slip to form NBC sources, the action of which would hide the activity of the initial BC sources.

The simulations give new results about dislocation dynamics at crack tips. Two-dimensional simulations indicate that when dislocation nucleation at the crack tip is easy, the materials toughness is controlled by the dislocation mobility. The faster the dislocations glide away from the crack region, the more dislocations are emitted at the source. The dislocation density in the plastic zone is higher for higher dislocation mobility (i.e. higher temperature) and can provide better shielding of the crack. This is why the activation energy for dislocation velocity and the activation energy derived from strain rate variation of the brittle to ductile transition are found to be identical, for a wide range of materials [8, 24, 25].

We might extrapolate from this two-dimensional analysis that the dislocation source configurations in three dimensions likely to provide the greatest shielding effect would be those giving the fastest emission rate. The simulations here show that this simple criterion does not always work; BC sources have the maximum emission rate but do not provide good shielding of the crack. The reasons for this lie in the use of both screw and edge components of the same dislocation loops in the three-dimensional simulations.

The dislocation emission rate is always controlled by the mobility of the slowest part of the dislocation loop. In the case of b.c.c. metals, the screw dislocations are much less mobile than the edge dislocations. The emission rate will be relatively high if the plastic zone is composed principally of edge dislocation segments. On the other hand, screw dislocations give higher shielding since they glide away from the crack region slowly and form a dense reverse pile up. These simulations, though simplified in many aspects, underline the complexity of this "competition" between the plastic zone shielding and the inhibition of the sources. This dynamical problem is strongly dependent on the exact three-dimensional geometry of the problem. The presence of the different dislocation types also has implications for the observation of the "dislocation free zone". A large dislocation free zone is observed in the BC case since the plastic zone is poor in screw dislocations and the edge dislocations in the plastic zone glide rapidly.

These simulations also give information about the effects of "dislocation microstructure" on the temperature and form of the brittle to ductile transition (BDT). The shielding associated with dislocations emitted from one source is strongly localized around this source. When the density of dislocation sources is low, even though the emission rate from each source is high, the crack may be unstable against external stress, since large areas of the crack between the sources are not efficiently shielded (as originally proposed by Hirsch *et al.* [6]). In materials with few dislocation sources at the crack tip, the transition to ductile behaviour is sudden, and depends on rapid dislocation multiplication from the few sources at the crack tip (as observed in experiments on silicon [3]). When a dense homogeneous source distribution is present along the crack tip, the crack stress intensity factor at all points on

the crack tip is efficiently reduced by the plastic zone shielding, as shown in Fig. 12. In this case, the transition is gradual, as is the case in b.c.c. metals.

Acknowledgements—We acknowledge the generous financial support of Nuclear Electric plc. It is a pleasure to acknowledge discussions with F. C Serbena, P. D. Warren, T. J. Marrow, J. Rigney and A. S. Booth.

REFERENCES

1. R. Thomson, *Solid State Physics* (edited by H. Ehrenreich and D. Turnbull), Vol. 39, p. 1. Academic Press, New York (1986).
2. J. Rice and R. Thomson, *Phil. Mag.* **29,** 73 (1974).
3. M. H. Ashbury and J. D. Embury, *Scripta metall. mater.* **19,** 557 (1985).
4. P. B. Hirsch, S. G. Roberts and J. Samuels, *Scripta metall. mater.* **21,** 1523 (1987).
5. P. D. Warren, *Scripta metall. mater.* **23,** 637 (1989).
6. P. B. Hirsch, S. G. Roberts and J. Samuels, *Proc. R. Soc. Lond.* **A421,** 25 (1989).
7. P. B. Hirsch and S. G. Roberts, *Phil. Mag.* **64,** 55 (1991).
8. S. G. Roberts, P. B. Hirsch, A. S. Booth, M. Ellis and F. C. Serbena, *Physica Scripta* **T49,** 420 (1993).
9. P. B. Hirsch and S. G. Roberts, *Scripta metall. mater.* **23,** 925 (1989).
10. Shu-Ho Dai and J. C. M. Li, *Scripta metall. mater.* **16,** 183 (1982).
11. M. Ellis, Doctoral Thesis, Oxford University (1993).
12. D. J. Capp, Doctoral Thesis, Oxford University (1975).
13. S. S. Lau, S. Ranji, A. K. Mukherjee, G. Thomas and J. E. Dorn, *Acta metall. mater.* **15,** 237 (1967).
14. T. Imura and H. Saka, *Mem. of Fac.*, Nagoya Univ, Japan. **28,** 55 (1976).
15. L. P. Kubin, G. Canova, M. Condat, B. Devincre, V. Pontikis and Y. Brechet, in *Non-linear Phenomena in Materials Science II* (edited by G. Martin and L. P. Kubin). Trans Tech Publication, CH-Aedermannsdorf (1992).
16. B. Devincre, Doctoral Thesis, University Paris-Sud Orsay, N° 2838 (1993).
17. B. Devincre and M. Condat, *Acta metall. mater.* **40,** 2629 (1992).
18. A. George and G. Michot, *Mater. Sci. Engng* **A164,** 118 (1993).
19. B. Devincre, *Solid State Com.* **93,** 875 (1995).
20. L. P. Kubin, *Rev. def. beha. mat.* **4,** 181 (1982).
21. J. Friedel, *Dislocations*. Pergamon Press, London (1964).
22. M. A. Loyola de Oliveira, Doctoral Thesis, Insitut National Polytechnique de Loraine (1994).
23. S. J. Zhou and R. Thomson. *J. Mater. Res.* **6,** 639 (1991).
24. C. St. John, *Phil. Mag.* **32,** 1193 (1975).
25. F. C. Serbena and S. G. Roberts. *Acta metall. mater.* **42,** 2505 (1994).